

---

## DAS trace location assignment for the CaMI.FRS Fibre loop

Kevin W. Hall and Don C. Lawton

### ABSTRACT

As our knowledge of the optical fibre loop at the Containment and Monitoring Institutes Field Research Station (CaMI.FRS) continues to evolve, we are able to assign  $x$ ,  $y$  and  $z$  coordinates to seismic traces recorded upon the loop using various interrogators. For example, gyroscope surveys conducted on observation wells 1 and 2 (OBS1 and OBS2) in the past year confirm that neither well is perfectly vertical. Using this updated information, we have built a trace geometry model that can be easily adjusted for varying trace spacings, uncertain cable lengths, fibre indices of refraction (actual and as used in interrogator software), and other unknowns. For downhole data with up- and down-going fibre, we may exploit symmetry by coarsely locating the bottom of the well using cross-correlation, fine-tuning using stack-power in sliding windows over a small trace range ( $\pm 5$  traces), and applying the geometry from our model. This strategy works well even for noisy shots, where cross-correlation by itself gives slightly varying answers from shot to shot. Quality control of observation well data thus far has been by inspection of interleaved up- and down-going DAS data sorted by true vertical depth (Figure 1) as well as stacks and residuals. Comparisons of straight and helical fibre data from the wells and the trench have not progressed beyond interleaving data sorted by true vertical depth or easting. Stacking will require a careful trace interpolation step to compensate for differing effective trace spacings.

### INTRODUCTION

The Containment and Monitoring Institute (CaMI) Field Research Site (FRS) has a CO<sub>2</sub> injection well (Injection) and two observation wells (OBS1 and OBS2) on the well lease (FIG. 1). In addition, there is a south-west to north-east oriented trench of approximately one metre depth roughly centered on OBS2. (Trench Fibre; FIG. 1). Borehole and trench optical fibres are connected in a continuous loop of about 5 km in length. Four junction boxes on wooden posts for fibre splices are present above the ground, one at each end of the trench (J.S and J.N), and one at each well (J.1 and J.2).

The fibre loop starts in a classroom trailer and continues through helical fibre in observation well 2 (OBS2H), straight fibre in observation well 2 (OBS2S), and straight fibre in observation well 1 (OBS1S) (FIG. 2). The loop then heads into the trench and travels from J.2 to the south end of the trench (J.S) as straight fibre (TrenchS1). Note that straight fibre in the trench is not identical to fibre found in OBS1S and OBS2S. The fibre loop continues the full length of the trench from south (J.S) to north (J.N) with helical fibre (TrenchH), and finally returns to junction box 2 (J.2) with straight fibre (TrenchS2). The loop terminates in the classroom trailer, and it is possible to acquire data in two opposite directions depending upon which fibre is attached to an interrogator in the classroom.

In order to process surface or borehole distributed acoustic sensing (DAS) data and compare to other datasets, we need to assign reliable spatial coordinates to each trace acquired on the fibre loop.

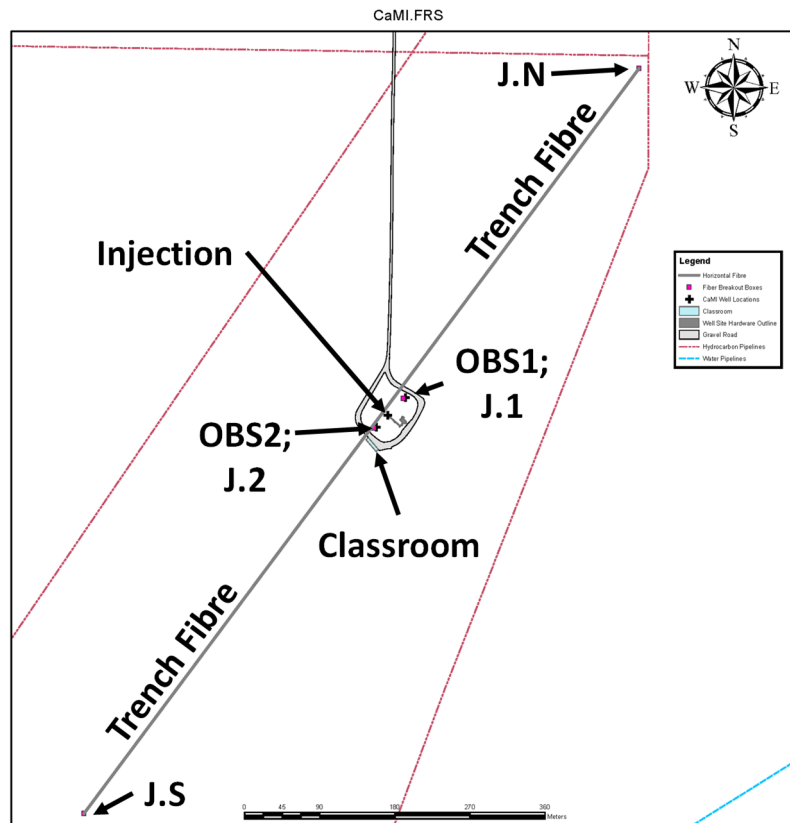


FIG. 1. Map view of Cami.FRS Fibre Loop showing locations of junction boxes (J.1, J.2, J.S, J.N) and locations of trench fibre and observation wells (OBS1, OBS2).

### Distance to splices on the fibre

Tap tests on fibre at splices in the junction boxes can confirm the order of borehole and trench segments in the loop but can be seen on tens of traces. Even if we were able to precisely locate a splice on the fibre with a tap test, it does not tell us precisely where fibre enters or exits the ground (well data) or becomes horizontal (trench data) (FIG. 2 and FIG. 3). Similarly, it is possible to very accurately measure the distance to each splice along the fibre loop, but these measurements suffer from the same limitations as tap tests when it comes to telling us which traces may be data traces. Both methods are affected by index of refraction and helical pitch.

### Previous work

It should be possible to find the traces closest to the bottom of the wells and the traces closest to a surface source near the trench by first break picking. Hall and Lawton (2018) had some success with this for well data but needed to use best-fit hyperbolae to the first break picks due to the fine trace-spacing (0.25 cm), jitter on helical data, and noisy data. This method gives no reliable information about where the well fibre enters or exits the ground. For trench data, manually picking the trace closest to a source from first-break picks is difficult because of the fine trace-spacing, broadside insensitivity of fibre data, jitter on helical data, asymmetry around the source point due to near surface anisotropy, and source noise.

Hall and Lawton (2018) attempted to locate fibre segment ends without any geometry constraints by summing the squares of trace amplitudes followed by a threshold. This method relies upon traces acquired on fibre that is above ground being significantly noisier than those that are in the ground and worked very well with the test dataset. However, it does not work very well for other datasets because some datasets are noisier than others, likely because of variations in wind noise from survey to survey. Additionally, noise from the junction boxes leaks into data traces when the source is far away from a junction box and signal leaks into junction box noise when the source is close to a junction box, likely due to gauge length averaging effects. This means that we are unable to consistently pick the same first and last segment traces from shot to shot using this method. Applying the threshold to all shots in a survey and averaging the results seemed promising but is inconsistent with newer information about the loop.

### Cable length

The length of fibre in any given junction box (d1,d4,d7,d10,d10,d12,d14; FIG. 2 and FIG. 3) is unknown. We cannot assume the length of fibre above ground is the same either side of each splice. We are also not certain what fibre was used between the junction boxes, helical or straight (eg. d7). In addition, we do not know the length of fibre in the wells used for splices at depth in the wells (d3, d6, d9).

However, we do have revised numbers for d2, d5, and d8 from well completion reports which appear to be reasonable (Table 1). We also have GPS data for locations of junction boxes J.2, J.S and J.N., where the horizontal distances from GPS can be modified by the known junction box geometry shown in FIG. 4. The GPS distance from J.S to J.N can be reduced by  $2 \times 0.7$  m, while distances from J.2 to J.S and J.2 to J.N can be reduced by 0.7 m each. The location of the red dot labeled ‘Trench Junction’ (FIG. 2 and FIG. 3) was determined by projecting the J.2 location perpendicularly onto a straight line between J.S and J.N. Cable lengths are summarized in Table 1.

### Helical fibre pitch

FIG. 5 shows an idealized helically wound fibre cable. A single wind of the helix can be represented by a right angle triangle (FIG. 5; bottom), where the portion of the helix representing the fibre lies along the hypotenuse (blue). It can now easily be shown that measured distances can be corrected using

$$d_{actual} = d_{software} \cos(\theta). \quad (1)$$

The pitch ( $\theta$ ) of the helix for the helical fibre at the CaMI.FRS is  $30^\circ$  (pers. comm.). To confirm, fifteen measurements were taken with a ruler on an admittedly non-pristine sample of the cable yielding an average  $d_{actual} = 10.68$  cm with a standard deviation of 0.37 cm. The radius of the helix is 1 cm, giving a circumference of  $2\pi$  cm. So,  $\theta = \text{atan}(2\pi/10.68)$ , or  $30.5^\circ$ .

Allowing our measured  $d_{actual}$  to vary by plus or minus one standard deviation gives us a range of pitches from  $29.63^\circ$  to  $31.35^\circ$ . A 1000.0 m of data from the interrogator will be between 854.0 and 869.2 m along the axis of the cable for this range of pitches. For the remainder of this report we will use exactly  $30^\circ$ , resulting in an actual cable length of 861.9

m for the current example. This equates to a 138 m error by the end of the fibre if helical pitch is not accounted for.

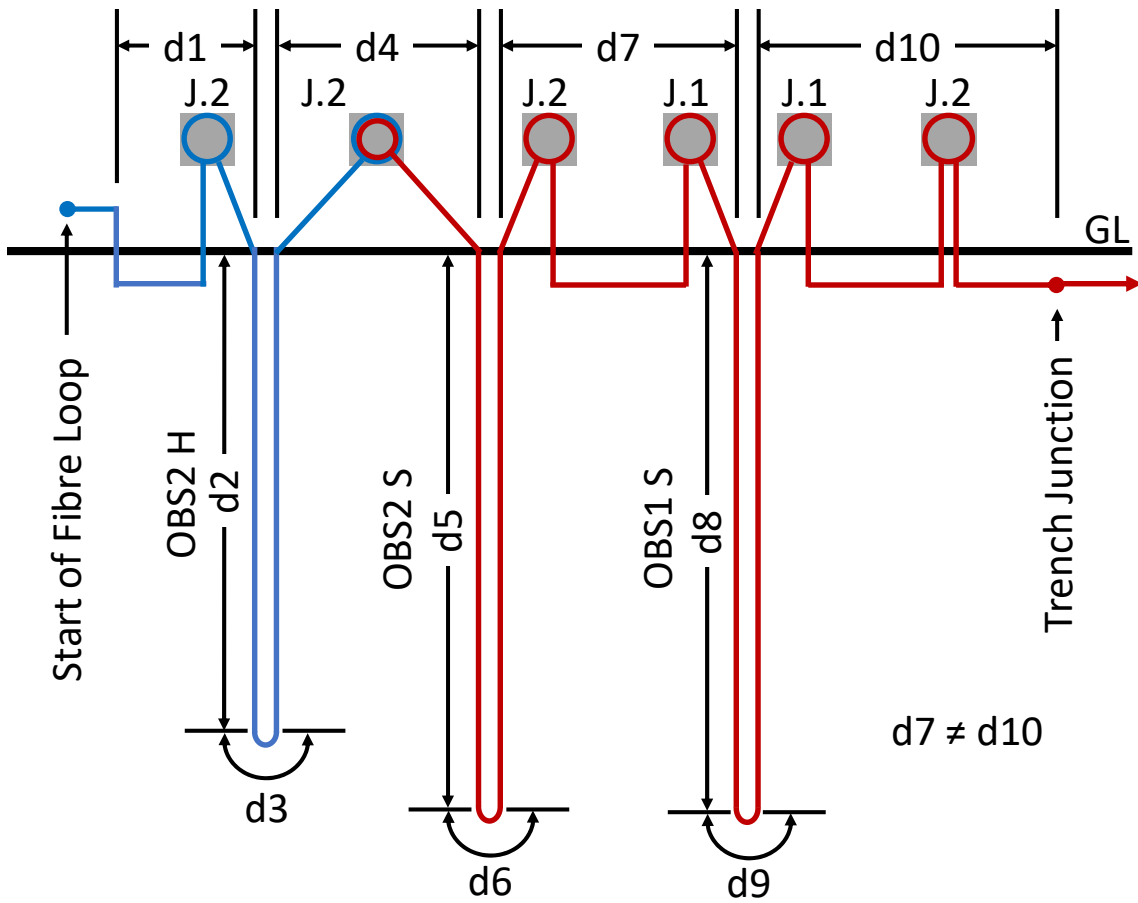


FIG. 2. Schematic of the observation well portion of the fibre loop with helical fibre in blue and straight fibre in red.

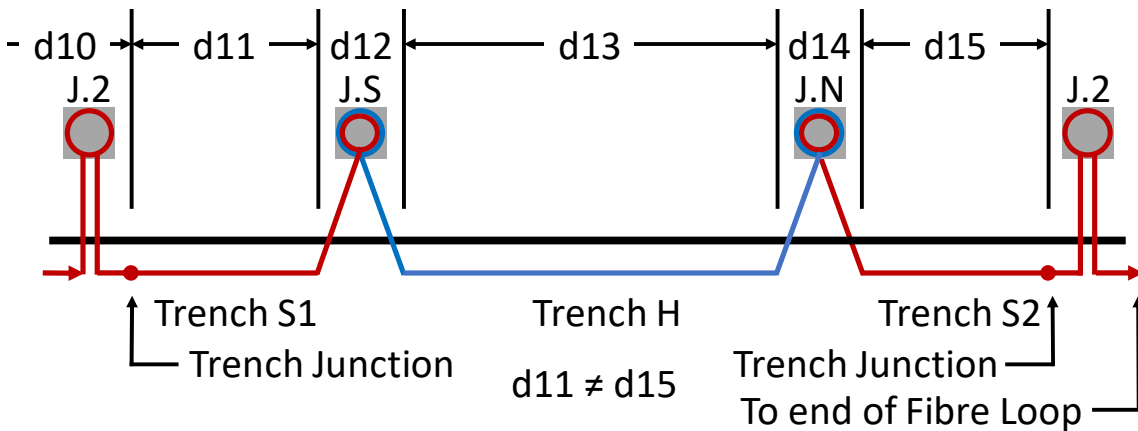


FIG. 3. Schematic of the trench portion of the fibre loop with helical fibre in blue and straight fibre in red.

Table 1. Cable lengths.

Segment	Data	Distance	Corrected Distance	Source
d2	OBS2H	Fibre to 334.43 mKB	329.53 mSurface	Schlumberger
d5	OBS2S	Fibre to 334.40 mKB	339.50 mSurface	Schlumberger
d8	OBS1S	Fibre to 348.10 mKB	343.20 mSurface	Schlumberger
d11	TrenchS1	577.37 m (J.2proj to J.S)	576.67	GPS
d13	TrenchH	1111.40 m (J.S to J.N)	1110.00 m	GPS
d15	TrenchS2	534.03 (J.N to J.2proj)	533.33	GPS

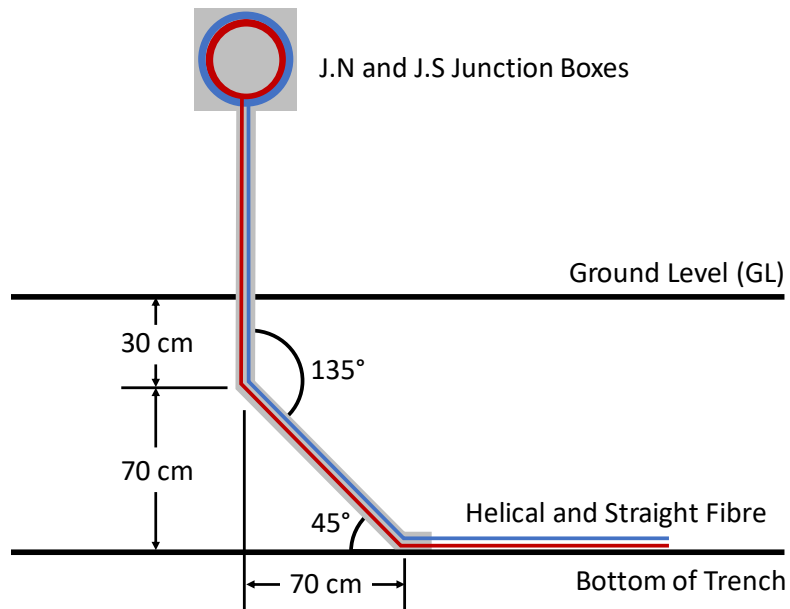


FIG. 4. Geometry of J.N and J.S fibre junction boxes.

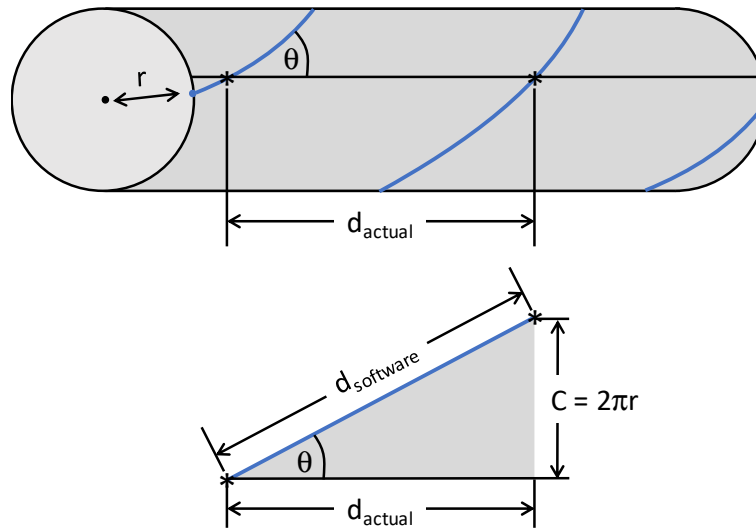


FIG. 5. Geometry of helically wound fibre where  $r$  is the radius of the helix,  $c$  is the circumference of the helix,  $\theta$  is the pitch,  $d_{software}$  is the distance along the fibre calculated by the interrogator, and  $d_{actual}$  is the desired distance along the cable.

### Index of refraction

There are three types of optical fibre in the fibre loop. We know that the index of refraction (IR) for the helical fibre is 1.467 at 1300 nm or 1.468 nm at 1500 nm (pers. comm.), but the IR for straight fibre in the observation wells and trench are unknown. The straight fibre in the trench is not the same as the straight fibre in the wells, and may have a different IR. Several operators have stated that they use an IR of 1.5 in the software if they do not know what the actual IR may be. Measured fibre distances depend on the time required for light to travel from one trace to the next, so we propose to correct the trace spacing using the following equations:

$$v = \frac{d}{t}, \text{ and } IR = \frac{c}{v}, \therefore t = \frac{d \cdot IR}{c}, \quad (2)$$

where  $d$  is distance (could be trace spacing),  $v$  is velocity,  $t$  is observed travel time,  $c$  is the speed of light in a vacuum and  $IR$  is the index of refraction. We may now create two equations for two different indices of refraction and set them equal knowing that the observed  $t$  is the same for both cases:

$$t_{observed} = \frac{d_{actual} \cdot IR_{actual}}{c} = \frac{d_{software} \cdot IR_{software}}{c}, \quad (3)$$

which leads to

$$d_{actual} = \frac{d_{software} \cdot IR_{software}}{IR_{actual}}. \quad (4)$$

Using Equation 4,  $d_{software} = 1000.0$  m obtained on fibre with  $IR_{actual} = 1.468$  using  $IR_{software} = 1.5$  in the interrogator yields an actual distance 1021.8 m. This is a  $\sim 22$  m position error at the far end of the fibre.

FIG. 6 shows data acquired on helical fibre (OBS2H) roughly centred on the bottom of the well and surface and bottom well locations overlain (see Method section, below). The top figure has two red downward pointing arrows that represent interpreted locations of junction box J.2 in the data (compare with left side, FIG. 2). Red and blue lines at the left and right of this figure show the calculated location of fibre traces where the fibre exits the ground at the top of well if we treat this data as straight fibre. The middle figure shows the result of applying a  $\cos(30^\circ)$  correction for helical pitch. Our calculated surface locations are now outside of the noisy traces we are interpreting to be junction box noise. The bottom figure shows the result of correcting for helical pitch as well as for index of refraction, where the actual IR is 1.468 and the interrogator was setup to use an IR of 1.5. Straight fibre examples in this report assume  $IR_{\text{software}} = IR_{\text{actual}} = 1.5$ .

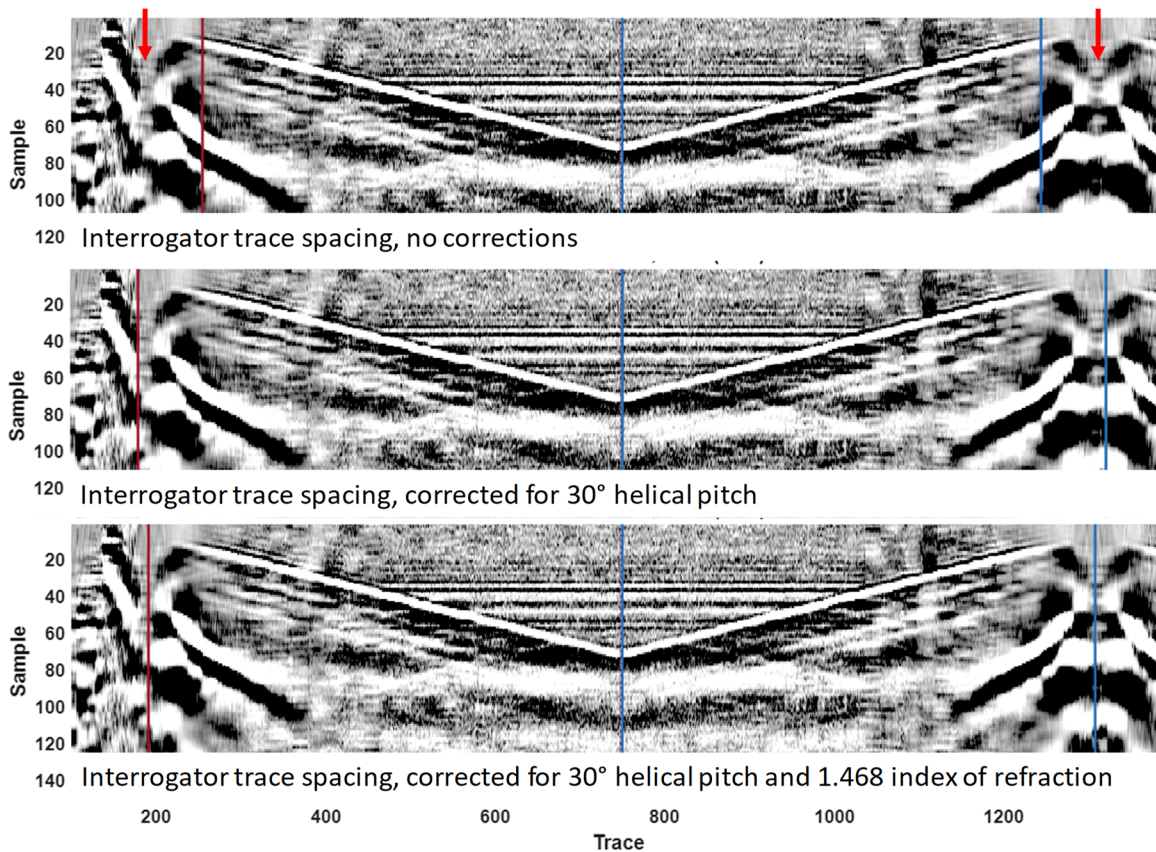


FIG. 6. Example of the effect of helical pitch and index of refraction corrections on trace geometry for helical fibre data in observation well 2 using a cable length 329.53 m (Table 1). Red arrows (top) show interpreted junction box locations (J.2). Blue lines (middle) show bottom of well location, red lines (left) and blue lines (right) show calculated surface locations.

## METHOD

Our latest strategy is to generate a geometry model by calculating the number of traces required for each fibre segment using all available information and then locate the optimal position for that trace window on the fibre loop data. The easiest way to do this is to overlay a calculated trace window plus some offset from the previous segment on the data (eg. FIG. 6) to position the trace geometry in roughly the correct position, and then tune the result.

### Well and trench coordinates

After accelerometers (Inova VectorSeis) inside casing in OBS2 showed that the well was not precisely vertical (Hall et al., 2018), gyroscope surveys were acquired in OBS1 and OBS2 in 2019 at a nominal 25 m sample spacing (black control points; FIG. 7a and FIG. 7b). The gyroscope survey in OBS2 confirmed that the well is deviated and gave us azimuthal information that was not available from the accelerometers. The bottom of OBS1 is displaced horizontally 2.7 m from the top. The bottom of OBS2 is displaced horizontally 11.25 m from the top. These numbers are not large for seismic, but the largest DAS trace spacing for all surveys conducted at the site to date is on the order of one meter. FIG. 7c shows a similar plot, but the control points are GPS locations for buried electrodes in the trench at a nominal 10 m trace spacing. Given these control points, we may linearly interpolate  $x$ ,  $y$  and  $z$  coordinates for each segment of the fibre loop (blue dots; FIG. 7) at the corrected trace spacing used for each interrogator. We now need to position this information on fibre data traces. In order to determine start and end traces for each fibre segment, we may exploit symmetries in the fibre loop

### Fibre loop symmetry

FIG. 8 shows a schematic of a typical shot gather, where blue lines represent direct arrivals and orange lines represent axes of symmetry that may be exploited in order to assign trace locations. FIG. 9 shows a corresponding source gather. Well symmetries Sy1, Sy2 and Sy3 represent the bottom of the observation wells. For now, we are going to assume that, 1) the closest fibre traces to the surface are at exactly at zero depth, 2) traces to the left and right of the splice are at exactly the same depths in the well, and 3) distances  $d_3$ ,  $d_6$  and  $d_9$  (FIG. 2) across the splices are equal to one trace interval. None of these assumptions are likely to be exactly true. In addition, helical and straight fibre data in observation well 2 (OBS2H and OBS2S) may be compared after accounting for differing amplitudes and actual trace spacings. Trench symmetries Sy4 and Sy5 (Figure 7) represent junction boxes J.S and J.N, and have two issues: 1) An unknown length of straight and helical fibre between horizontal fibre in the trench and splices in J.N and J.S, and 2) different trace intervals.

The best way that we have found to locate the deepest traces in a well is to coarsely tune the bottom well location by cross-correlate small trace panels on opposite sides of Sy1, Sy2 and Sy3 after interpreting the approximate location of these symmetries in the data. Cross-correlating using a single trace works less well due to noise. In fact, cross-correlating panels gives us an answer that varies by up to 3 or 4 traces from shot to shot due to noise but does resolve up to several hundreds of traces of error in the initial position. Fine-tuning by folding well data across the bottom well location given by cross-correlation and comparing stack power in sliding windows over a small trace range ( $\pm 5$  traces from the

cross-correlation result) gives us a consistent answer from shot to shot regardless of noise or type of fibre.

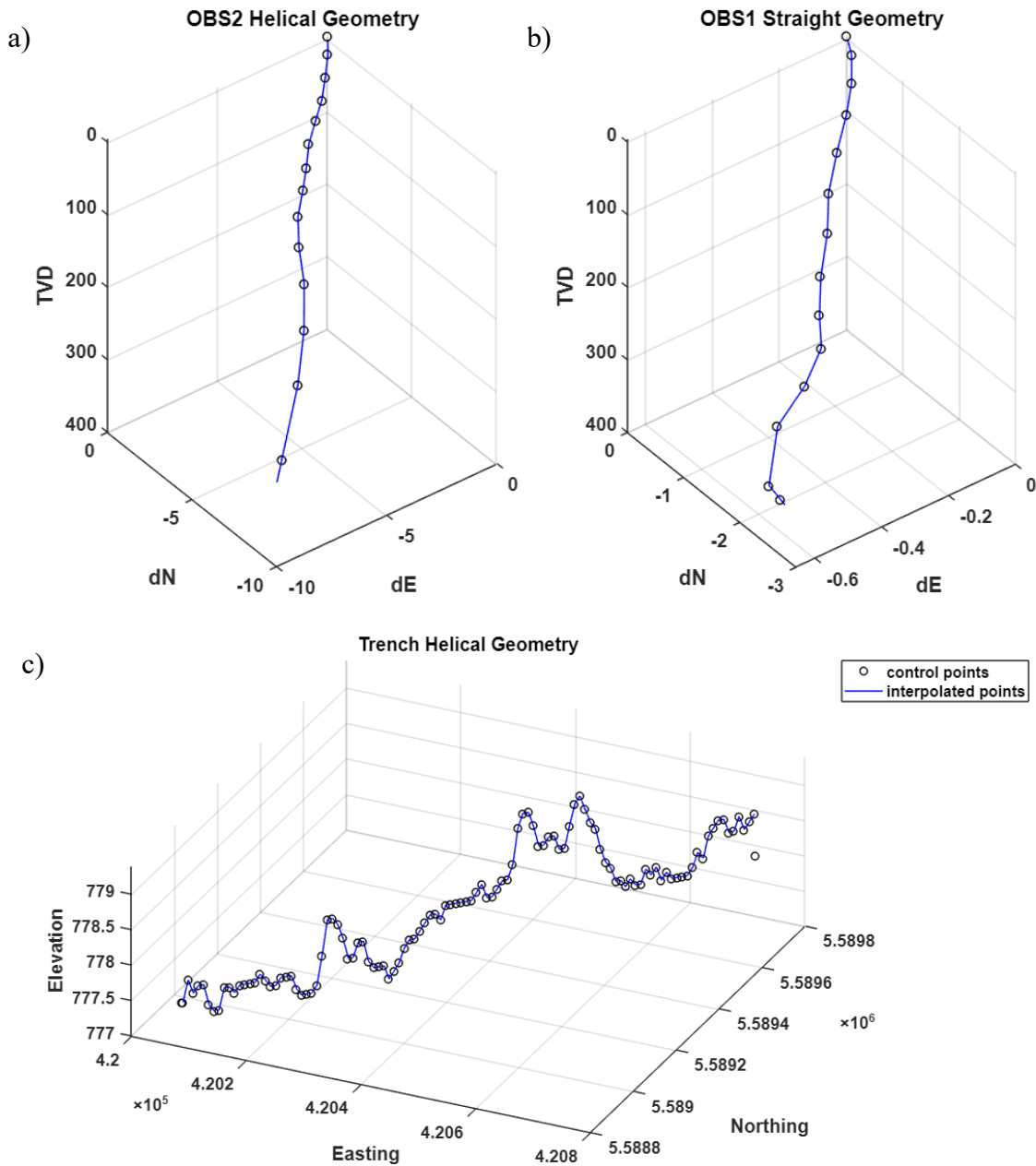


FIG. 7. Examples of well and trench geometries. Black control points are from gyroscopic surveys (a and b) in the wells or GPS locations for electrodes in the trench (c). Blue dots are linearly interpolated trace locations based on fibre cable lengths and corrected trace spacings.

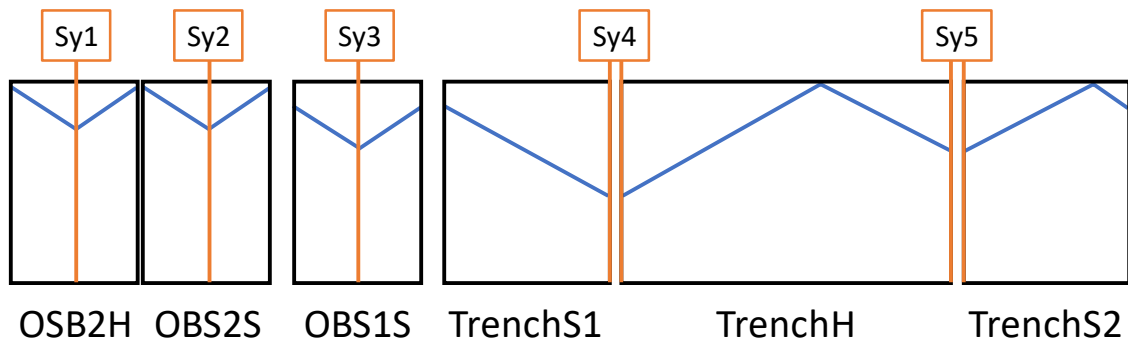


FIG. 8. Schematic showing symmetries that can be exploited for geometry assignment.

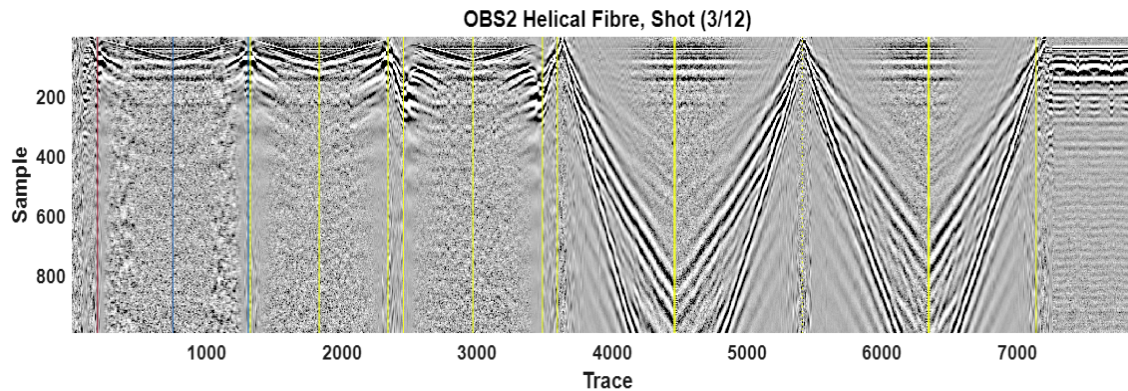


FIG. 9. A sample source gather for comparison with FIG. 8. Red, blue and yellow lines represent trace windows derived from the geometry model after coarse and fine-tuning.

Cross-correlations across Sy4 and Sy5 after stretching straight data to match helical data distances have been unsuccessful to date. Like the sum-of-squares of amplitudes idea (Hall and Lawton, 2018), we attempted cross-correlations using a single trace to define trace-windows corresponding to the width of the gaps at Sy4 and Sy5. The assumption here is that noise in junction box traces is coherent and will correlate with other nearby noisy traces better than they will with a data trace. Unfortunately, this method also suffers from gauge length averaging effects where noise bleeds into data and vice versa. For now, we are reduced to centering the trace window between noise bands from the junction boxes, and then interleaving with data from the straight fibre segments followed by visual inspections to confirm.

## RESULTS

FIG. 10 through FIG. 15 show mean stacks and residuals across Sy1, Sy2 and Sy3 for OBS2H, OBS2S and OBS1S for the source gather shown in FIG. 9 after assigning trace geometry and sorting by receiver depth. We feel these results are the best we can do without interpolating traces. These images are only diagnostic for our choice of the deepest traces in each well. They do not tell us anything about the correctness of our geometry and in particular our corrections for helical pitch and index of refraction. FIG. 16 shows data from helical and straight fibre in OBS2 after geometry assignment and sorting the traces by receiver depth. This image gives us some confidence that we are on the right track.

FIG. 17 shows trench straight fibre segments (TrenchS1 and TrenchS2) interleaved with the helical fibre segment (TrenchH) after assigning geometry and sorting by easting. Jitter amplified by screen aliasing near the source and at the north and south ends of the trench in this image imply that we do not have the helical pitch and index of refraction corrections exactly right. To a lesser extent, this effect can also be seen on the borehole data, where jitter increase towards the surface (left side; FIG. 16).

## DISCUSSION

Given updated information on borehole trajectories and cable lengths in the boreholes, we have been able to linearly interpolate  $x$ ,  $y$  and  $z$  coordinates along these trajectories and determine the number of traces of a DAS dataset required to accommodate this information. This requires correcting the trace spacing reported by each vendor for the helical pitch of helically wound fibre, as well as the index of refraction (IR) of the fibre if the value used in interrogator software does not match the actual IR of the fibre.

For downhole data with up- and down-going fibre, we may exploit symmetry by coarsely locating the bottom of the well using interpretation, cross-correlation, and then fine-tuning using stack-power in sliding windows over a small trace range ( $\pm 5$  traces), and applying the geometry from our model. Trench data segments are thus far matched to geometry trace windows by centering the trace window between noisy bands of traces where the fibre is above ground. Comparisons of straight and helical fibre data from the wells and the trench have not progressed beyond interleaving data sorted by true vertical depth or easting. Stacking to compare straight and helical fibre data will require a careful trace interpolation step to compensate for differing effective trace spacings.

Results to date show that our corrections for helical pitch and index of refraction may not be exactly correct, as helical and straight data show progressively worse jitter from side to side when interleaved.

## FUTURE WORK

We need to devise a better method for landmarking the geometry trace windows on trench fibre data. We also need to further constrain our geometry model by obtaining the index of refraction of the two types of straight fibre in the fibre loop, which are currently unknown to us. This information should help us resolve mismatches we observe on interleaved straight and helical fibre data.

## ACKNOWLEDGEMENTS

The authors would like to thank and all CREWES sponsors and CaMI.FRS JIP subscribers. This work has been partially funded by NSERC under grant CRDPJ 461179-13 and the Canada First Research Excellence Fund (CFREF).

## REFERENCES

Hall, K.W., and Lawton, D.C., 2018, Optical fibre data registration: CREWES Research Report, **30**, 12p.

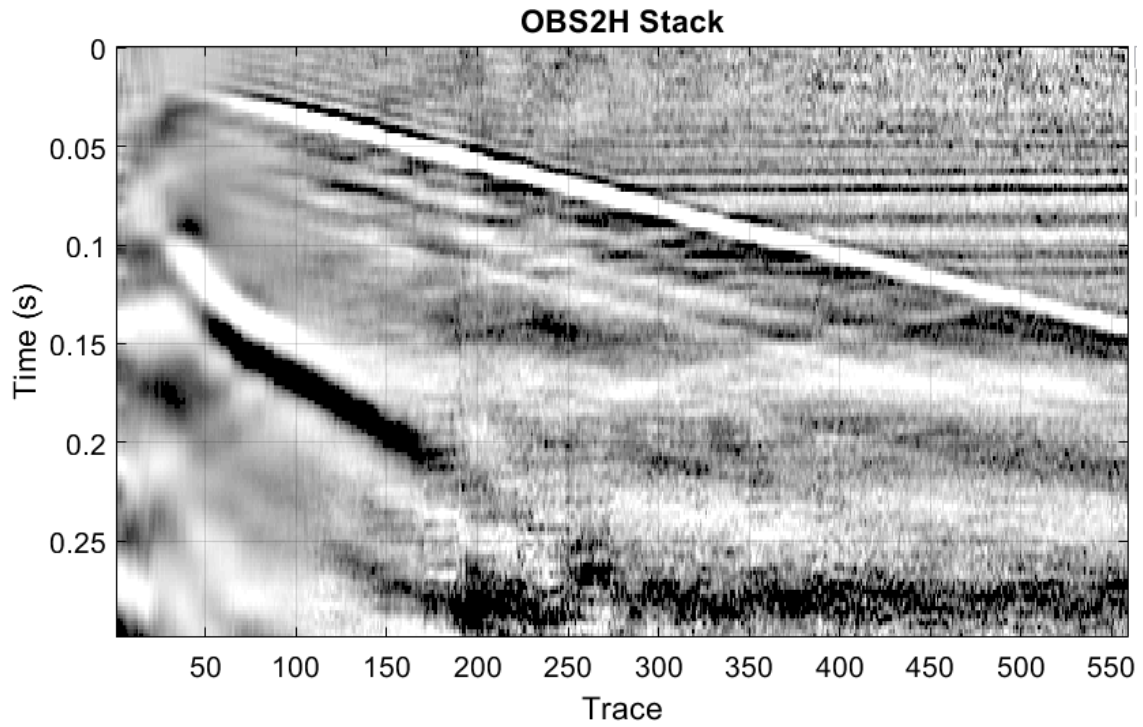


FIG. 10. Observation well 2 helical fibre stack.

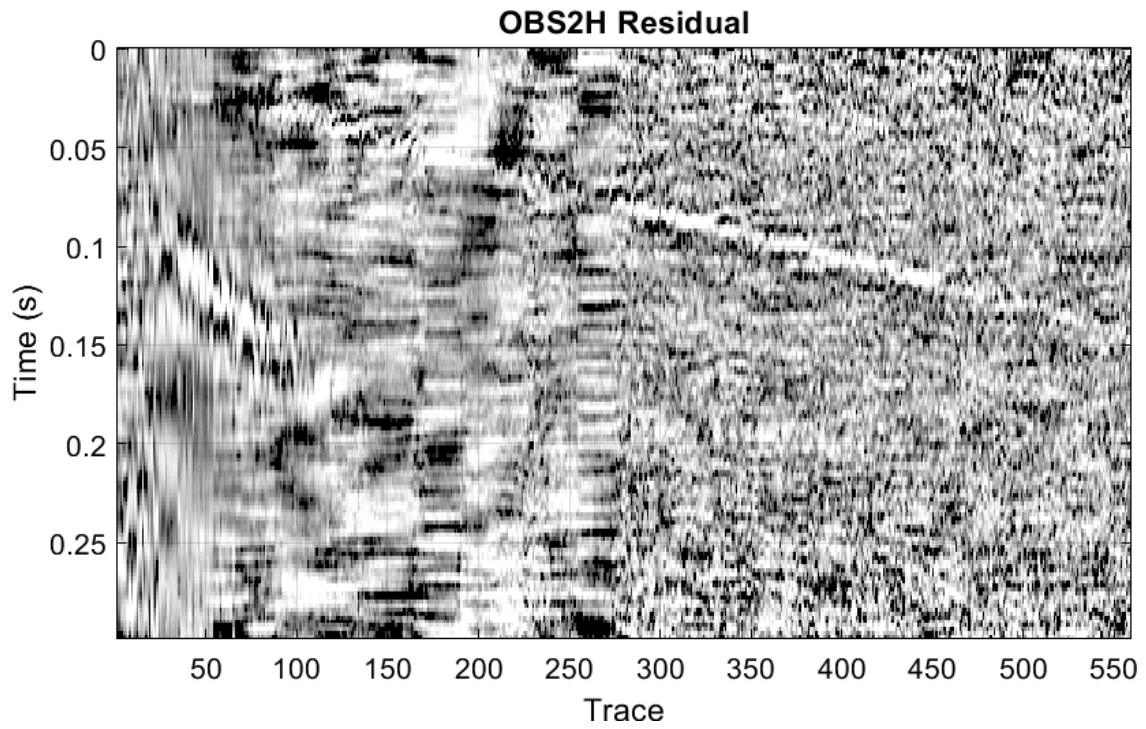


FIG. 11. Observation well 2 helical fibre residual.

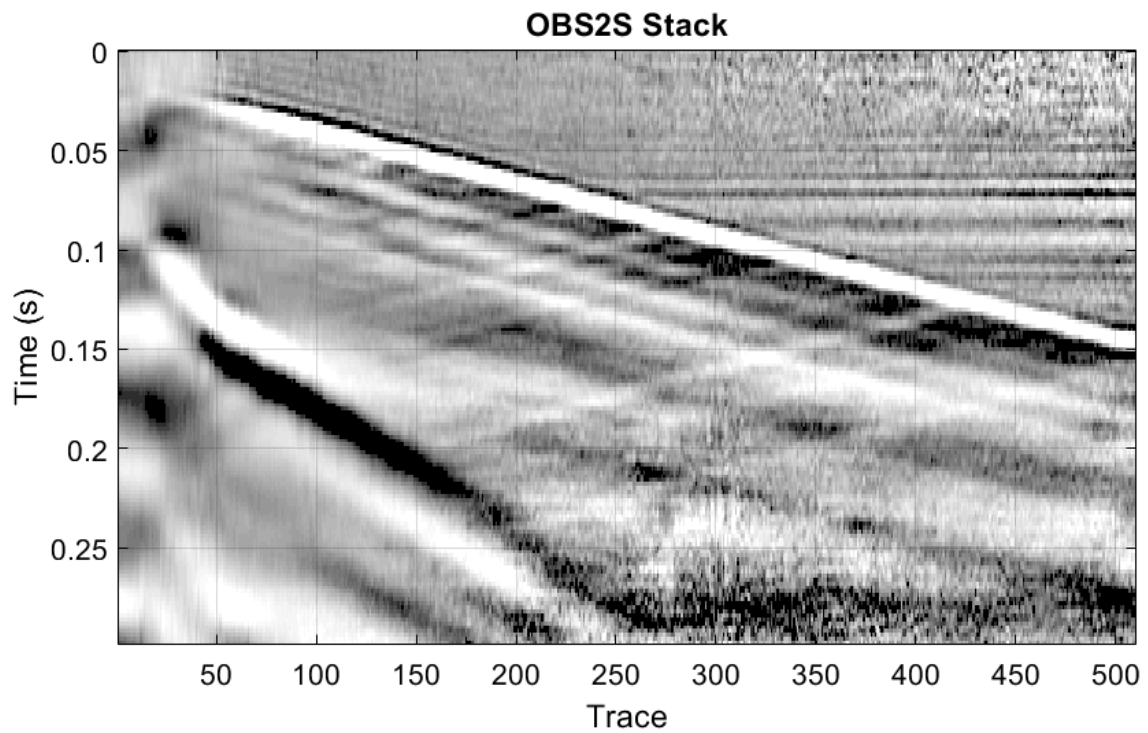


FIG. 12. Observation well 2 straight fibre stack.

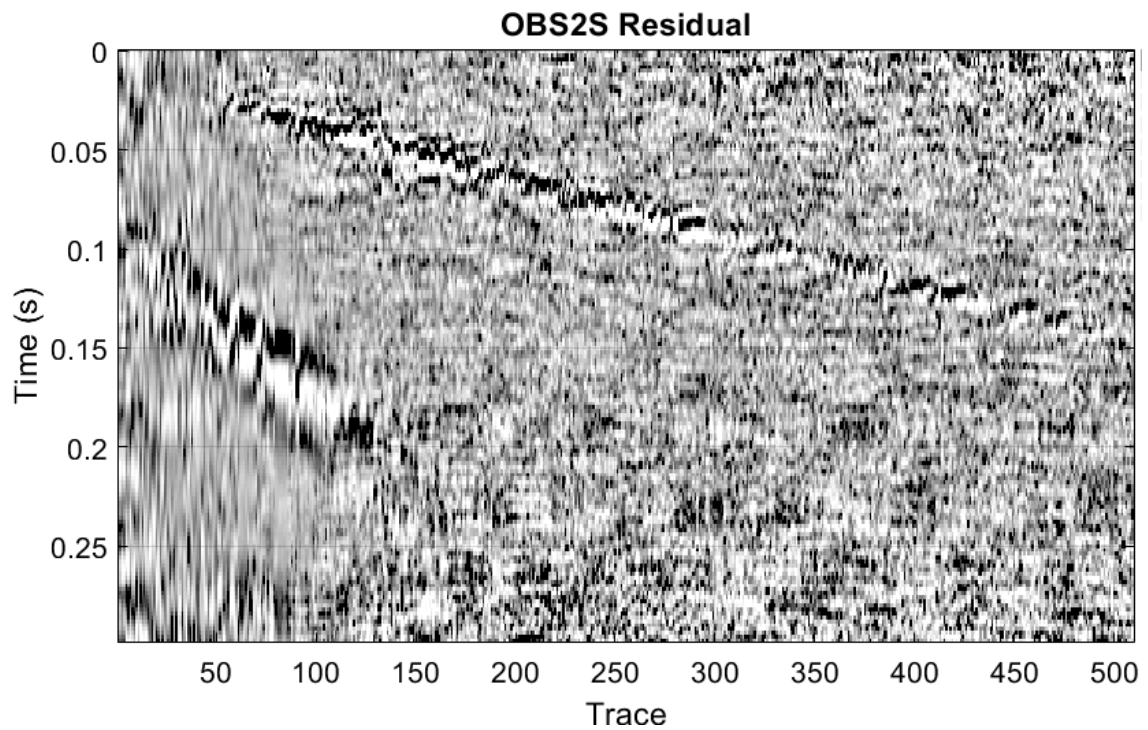


FIG. 13. Observation well 2 straight fibre residual.

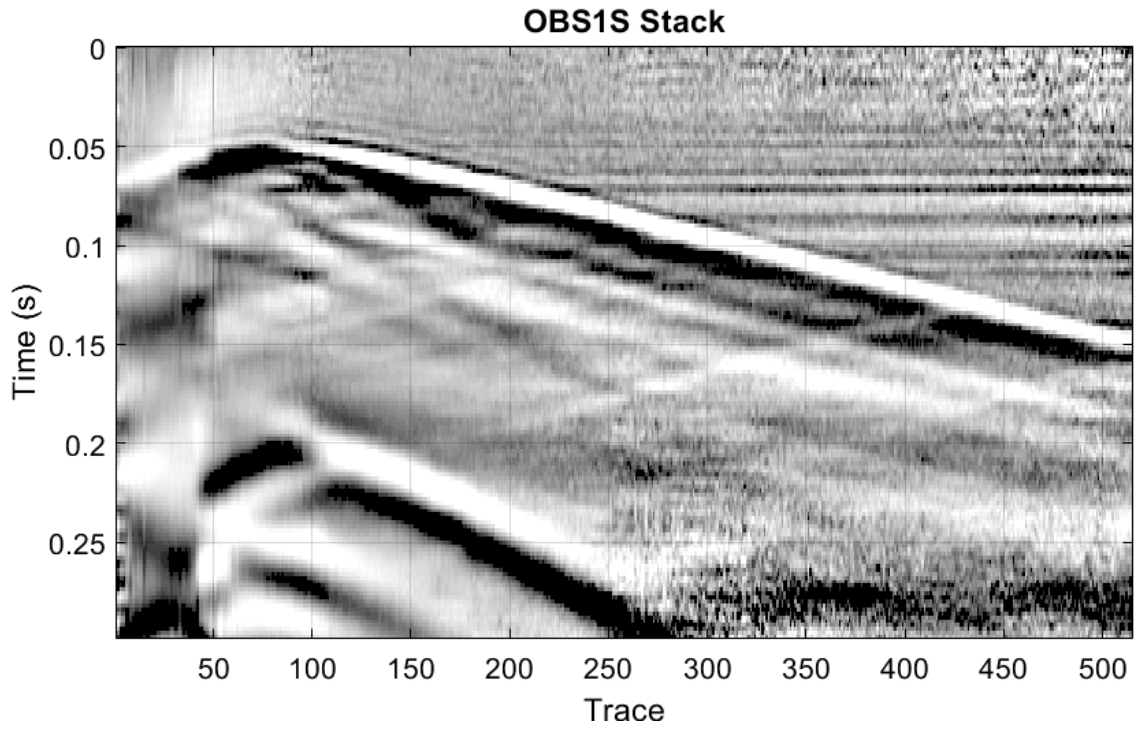


FIG. 14. Observation well 1 straight fibre stack.

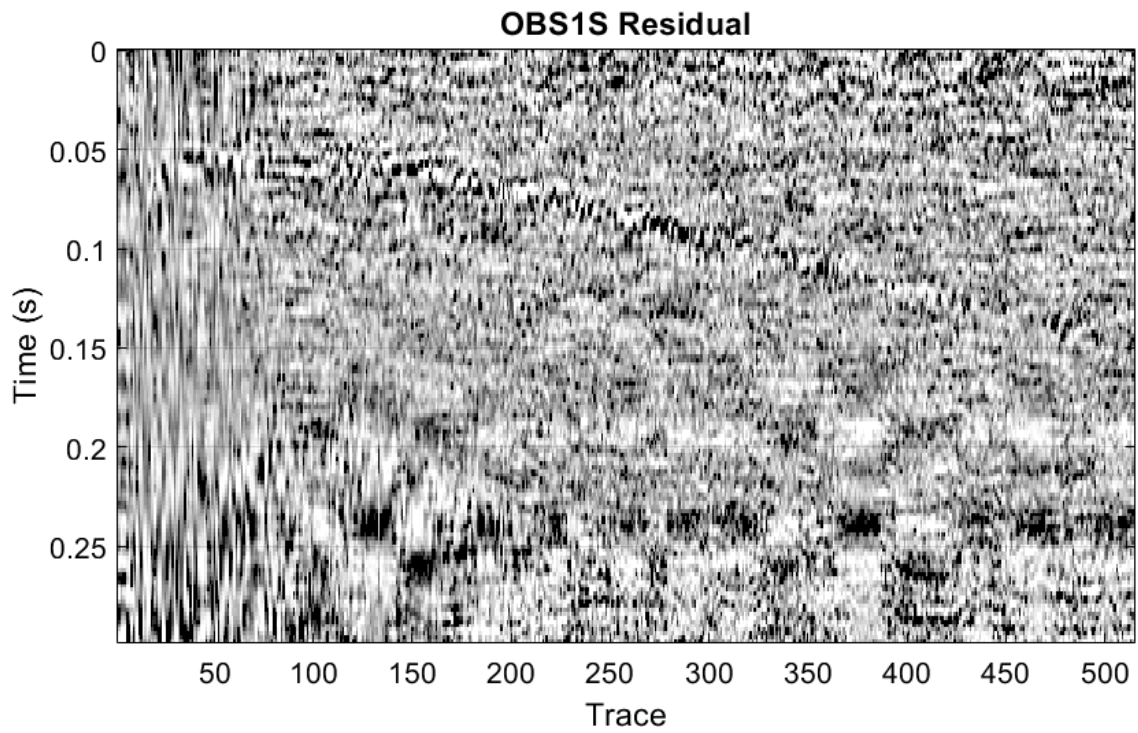


FIG. 15. Observation well 1 straight fibre residual.

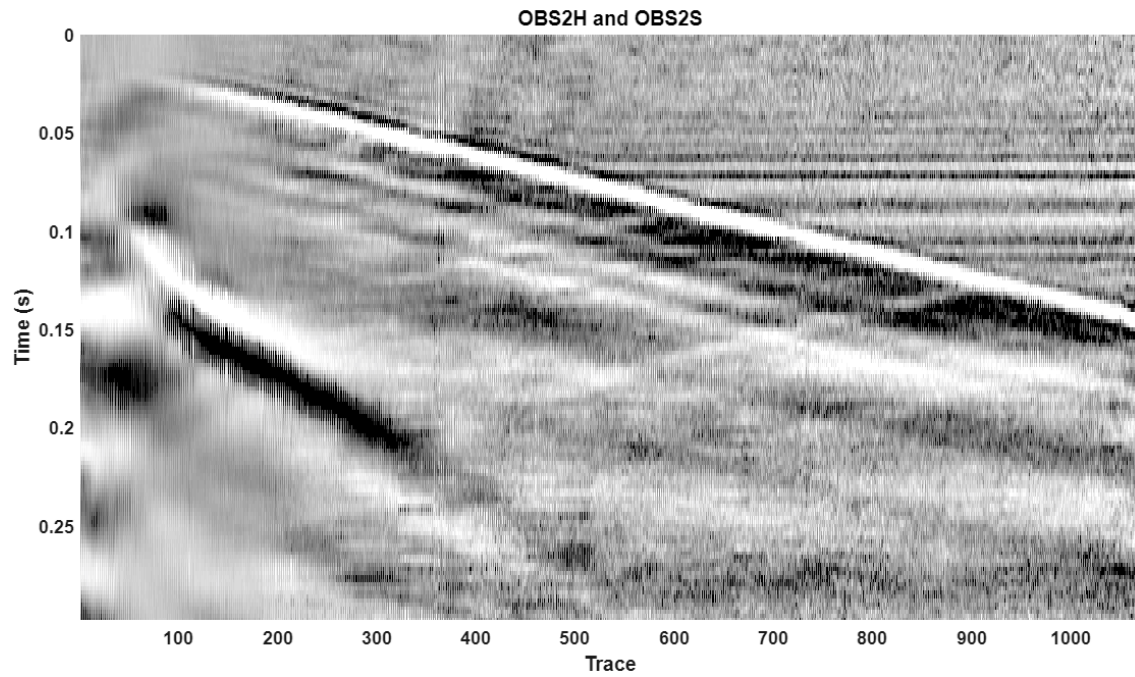


FIG. 16. Observation well 2 helical and straight fibre sorted by true vertical depth.

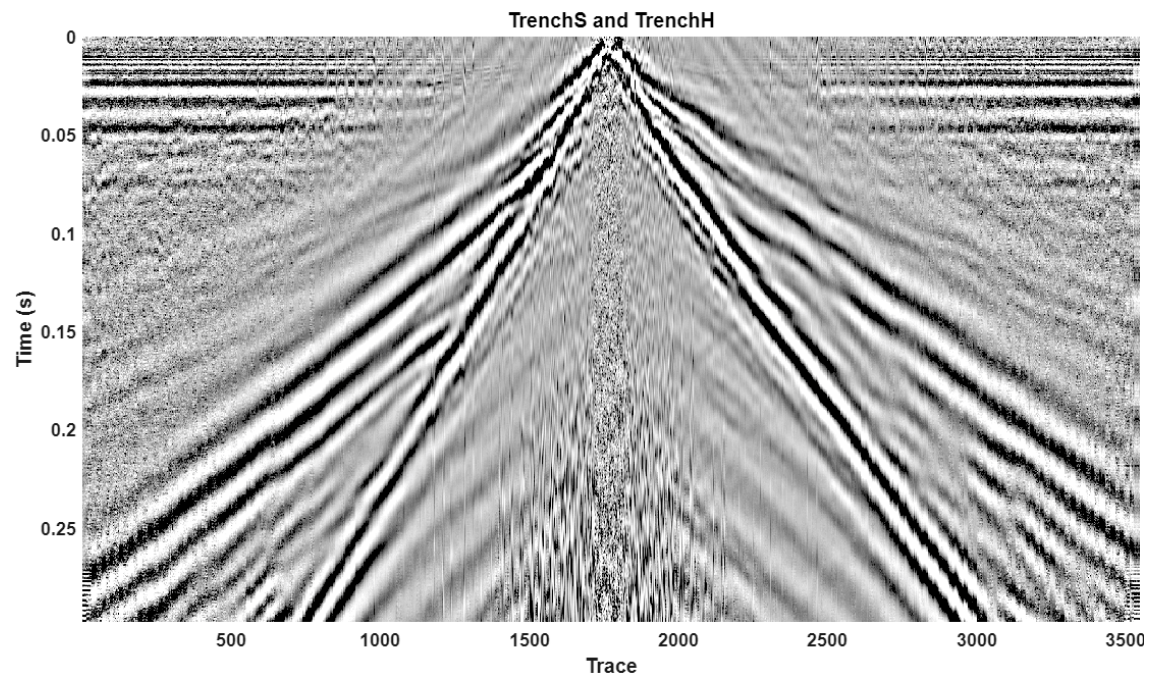


FIG. 17. Trench helical and straight fibre data sorted by easting for trench segments S1, H and S2.